Power Electronic Interface with an Adaptive MPPT Technique for Train Suspension Energy Harvesters

Luigi Costanzo, Teng Lin, Weihan Lin, Alessandro Lo Schiavo, *Senior Member, IEEE,* Massimo Vitelli and Lei Zuo

***Abstract*—An electronic interface for the maximization of the power extraction from train suspension energy harvesters is presented. It is made up of a passive rectifier and a DC/DC converter equipped with a digital control unit that implements a novel maximum power point tracking technique. It can settle the voltage at the rectifier output to its optimal value, despite the time-varying train suspension vibrations. By exploiting the measurement of the generator speed, the proposed technique is able to almost instantaneously reach the maximum power point, allowing a power extraction higher than the widely used perturb and observe algorithm. Moreover, the proposed technique is equipped with an adaptive control for ensuring the power maximization despite the tolerances and time-variability of the system parameters. Experimental results validate the theoretical analysis and confirm the superior performance of the proposed interface.**

***Index Terms*—Train Suspension Energy Harvesters; Maximum Power Point Tracking; Perturb and Observe.**

I. Introduction

THE transportation safety and efficiency of freight wagons can be significantly improved by equipping them with on board sensors for continuous monitoring and tracking. The lack of electricity in freight cars, needed for powering on board sensors, can be overcome by resorting to the harvesting of otherwise wasted energy [1]-[3]. As a significant amount of energy is usually dissipated in railcar suspensions through oil shock absorbers or frictional dampers, a large variety of Train Suspension Energy Harvesters (TSEH) have been proposed in the literature [3]. Examples are linear electromagnetic harvesters, where magnets move linearly with the train suspension inside coils [4]-[5], or rotary electromagnetic harvesters, which are able to convert the linear motion of the suspension into a bidirectional [6] or a unidirectional rotation [7] of an electromagnetic generator. The last ones are based on Mechanical Motion Rectifier (MMR) systems that increase the efficiency by allowing the generator to always rotate in the same direction [7]-[17].

Whatever may be the linear-to-rotary conversion principle, all the rotary harvesters exploit an electromagnetic generator to convert the mechanical energy into electrical energy [6]-[17] and, thus, require the rectification of the output AC voltages. In the most widely used AC/DC converter, i.e. the diode bridge rectifier [18]-[21], the power extracted from the harvester is strictly linked to the value of the rectifier output voltage [22]-[25]. In particular, an optimal voltage exists that leads to the maximization of the harvested power, and its value is time varying with the train suspension vibrations.

Since the maximum power transfer theorem allows the prediction of the optimal matched load only for linear circuits [26], recently resonant harvesters have been investigated in order to identify the optimal voltage at the output of the non-linear converter [22]-[23]. Unfortunately, the non-resonant nature of TSEHs and their non-sinusoidal operating conditions do not allow the application of the above concepts. As far as the authors know, the investigation of the optimal operating conditions and of the dynamic tracking of the Maximum Power Point (MPP) in TSEHs loaded by passive bridge rectifiers is addressed in this paper for the first time.

In energy harvesting applications, the most widely used Maximum Power Point Tracking (MPPT) technique is the Perturb and Observe (P&O) [24]-[25]. It is based on a "Hill Climbing" algorithm that tries to find the peak of the hill in a blind way, i.e. without any global information on the system, just exploiting the local information on the extracted power. Thus, the P&O algorithm, operating step by step, takes a time to reach the MPP that is significantly greater than the system settling time. This is not acceptable in applications with quickly time-varying MPPs, as it happens in TSEHs due to the time variability of the train suspension vibrations. Moreover, the effectiveness of the P&O technique is strictly related to the design parameters that must be properly and accurately chosen as a function of the actual characteristics of the energy source [24]-[25], which are quite unpredictable in TSEHs applications.

Manuscript received March 04, 2020; revised April 15, 2020; accepted July 07, 2020. This work was partially supported by "VALERE: VAnviteLli pEr la RicErca" research program by Università degli Studi della Campania "Luigi Vanvitelli". The authors would like to thank the partial funding support from NSF #1738689. Co-author T. Lin conducted the harvester design in his spare time (while employed at Allegiant Health, NY), W. Lin supported the system integration and lab test, L. Costanzo and A. Lo Schiavo designed the power electronic interface with adaptive MPPT technique, M. Vitelli and L. Zuo supervised the research and tests. We also thank former PhD students Dr. Yu Pan and Dr. Hongjip Kim for discussions on the harvester design and assembly.

(Corresponding Author: Luigi Costanzo, +39 0815010212).

L. Costanzo, A. Lo Schiavo and M. Vitelli are with the Department of Engineering, Università degli Studi della Campania "Luigi Vanvitelli", Aversa (CE), 81031, Italy, (e-mail: luigi.costanzo@unicampania.it, alessandro.loschiavo@unicampaia.it, massimo.vitelli@unicampania.it).

T. Lin, W. Lin and L. Zuo are with the Center for Energy Harvesting Materials and Systems (CEHMS), Virginia Tech, Blacksburg (VA), 24061, USA (email: leizuo@vt.edu).

In order to overcome the above limits of the P&O technique, a power electronic interface featured with a novel MPPT technique for TSEHs is presented in this paper. Such a MPPT technique, which is named Speed Driven Adaptive (SDA), allows a real-time direct estimation of the MPP, by exploiting the measurement of the generator speed, which is usually available in three-phase brushless electromagnetic generators. Thus, the SDA technique ensures a maximum power extraction, despite the possible time variations of the train suspension vibration characteristics. Moreover, the SDA technique implements a dynamic adaptive control to handle the tolerances and time variability of the parameters of the controlled system. Experimental results, obtained with reference to the highly efficient TSEH presented in [7], demonstrate the ability of the proposed SDA MPPT technique to track the MPP without errors in presence of fast time-varying generator speeds. Such results also show the advantages of the proposed SDA technique compared to the widely used P&O MPPT technique.

II. Train Suspension Energy Harvester

The TSEH shown in Fig. 1(a) [7], is an electro-mechanical system that is able to convert the mechanical energy associated with the bi-directional vibration between the bogie and the railcar body of the train into electricity. As shown in Fig. 1(b), it is composed of a rack, a pinion gear integrated with a shaft, an enclosed gearbox acting as MMR, a planetary gearhead and a three-phase brushless electromagnetic generator with a flywheel. In particular, the MMR converts the bi-directional rotation of the pinion shaft into a unidirectional rotation of the gearhead shaft and allows the improvement of the energy harvesting efficiency and the reduction of the impact force during transmission.

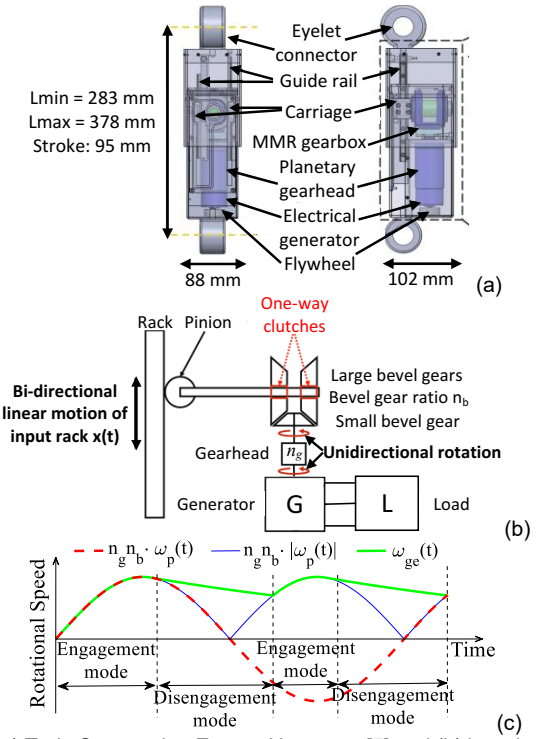

Fig. 1. (a) Train Suspension Energy Harvester [7] and (b) its schematic representation. (c) Engagement and disengagement modes in case of sinusoidal displacement.

The MMR gearbox is composed of two large bevel gears connected to the pinion gear shaft by means of two one-way clutches. The two large bevel gears are connected to the gearhead shaft through a small bevel gear. Due to the presence of the two one-way clutches, during the bi-directional rotation of the pinion gear shaft, the small bevel gear can be driven at most by one of the two large bevel gears that is, the one whose one-way clutch is engaged with the pinion gear shaft. The two large bevel gears are mounted so that the small bevel gear rotates always in the same direction. The operating mode named "Engagement mode" takes place when one of the two large bevel gears is engaged with the pinion gear shaft so that the input torque is transmitted from the pinion gear shaft to the gearhead shaft. In this operating mode, the speed ω_p of the pinion gear shaft is equal to the speed of one of the two large bevel gears. When ω_p decreases too fast, both the one-way clutches result disengaged from the pinion gear shaft and no torque is transmitted from the pinion shaft to the generator, which as shown in Fig. 1(c), is allowed to freely rotate faster due to the rotary inertia. This operating mode is named "Disengagement mode". The equations modelling the system operations are different in the engagement and disengagement modes and will be presented in the sequel. The detailed analysis of the TSEH and the electromechanical energy conversion process can be found in [7], [15]-[17], [21].

A. Engagement Mode

In the engagement mode, the speed of the generator shaft is equal to the rectified speed of the pinion, increased by the gearhead and bevel gears ratio, as shown in Fig. 1(c). If $x(t)$ is the displacement of the suspension vibration and r_p the pinion gear radius, the pinion gear shaft speed can be written as $\omega_p(t) = \dot{x}(t)/r_p$, neglecting backlash and compliance [7]. The small bevel gear speed can be expressed as $\omega_s(t) = n_b \cdot |\omega_p(t)|$, where n_b is the transmission ratio from the large bevel gears to the small bevel gear. Moreover, if n_g is the planetary gearhead transmission ratio, it is possible to write the generator speed as

$$\omega_{ge}(t) = n_g \cdot \omega_s(t) = n_g \cdot n_b \cdot |\omega_p(t)| \quad (1)$$

In this operating mode, the torque is transmitted from the pinion shaft to the generator shaft and the following mechanical equation holds

$$T_{ext}(t) = T_{ge}(t) + B_{ge} \cdot \omega_{ge}(t) + J_{tot} \cdot d\omega_{ge}(t)/dt \quad (2)$$

where T_{ext} is the torque driving the generator shaft, B_{ge} is the rotary damping coefficient of the generator and J_{tot} is the total rotary inertia of the generator and of the flywheel. Moreover, T_{ge} is the resistive torque associated with the electrical currents of the three-phase generator and it can be written as

$$T_{ge}(t) = \sum_{k=1}^{3} v_{ge-k}(t) \cdot i_{ge-k}(t) / \omega_{ge}(t) = \\ = p_{ge}(t) / \omega_{ge}(t) \quad (3)$$

where $v_{ge\text{-}k}$ and $i_{ge\text{-}k}$ are the k-th phase voltage and current, respectively. The voltage $v_{ge\text{-}k}$ is given by

$$v_{ge-k}(t) = k_e \cdot \omega_{ge}(t) \cdot sin\left[\theta_{ge}(t) + \frac{2(k-1)\pi}{3}\right] \quad (4)$$

where

$$\theta_{ge}(t) = \int_0^t n_p \cdot \omega_{ge}(\tau)\, d\tau \qquad (5)$$

k = 1, 2 and 3 is the phase number, k_e is the generator voltage constant and n_p is the number of generator pair poles. The currents $i_{ge\text{-}k}$ can be calculated from the following system

$$\begin{aligned} v_{ge-k}(t) - v_{ge-(k+1)}(t) - v_{load-k}(t) + v_{load-(k+1)}(t) = \\ = R_{ge} \cdot \left[i_{ge-k}(t) - i_{ge-(k+1)}(t)\right] + \\ + L_{ge} \cdot \left[di_{ge-k}(t)/dt - di_{ge-(k+1)}/dt\right] \end{aligned} \qquad (6)$$

where $v_{load\text{-}k}$ is the k-th phase voltage across a wye connected load, R_{ge} and L_{ge} respectively are the resistance and inductance of the generator's phase coils.

B. Disengagement Mode

When the train suspension motion reduces and, consequently, the pinion gear speed decreases, the MMR disconnects the pinion shaft from the generator shaft. As shown in Fig. 1(c), in this operating mode the generator speed is greater than the pinion gear speed, increased by the gearhead and bevel gear ratios, i.e. $\omega_{ge}(t) > n_g \cdot n_b\, |\omega_p(t)|$. The generator speed can be calculated by solving the mechanical equation

$$0 = T_{ge}(t) + B_{ge} \cdot \omega_{ge}(t) + J_{tot} \cdot d\omega_{ge}(t)/dt \qquad (7)$$

where T_{ge} is still given by (3)-(6).

It should be noted that, differently from the engagement mode, in the disengagement mode the generator speed ω_{ge} is not driven by the mechanical displacement $x(t)$. According to (7), ω_{ge} depends on the electrical torque T_{ge}, which in turn depends on the power delivered to the electrical load, i.e. on the extracted power. Moreover, it is worth noting that, according to (7), for a given electrical load, the greater the inertia J_{tot} the slower is the decrease of the speed ω_{ge}. Thus, in order to maximize the power delivered to the load in the disengagement mode, it is desirable to have a large inertia J_{tot}. This condition, in turn, leads to an almost constant generator speed.

III. AC/DC Conversion Analysis

The most suitable choice to rectify the three-phase AC output voltage of the generator is a diode bridge rectifier, due its simplicity and low losses [18]-[20]. Since, the power extracted from the TSEH is a function of the voltage V_{DC} at the output of the rectifier [21], the value of V_{DC} that allows the extraction the maximum power is analytically predicted. The TSEH loaded by a diode bridge rectifier is modelled by means of the equivalent circuit shown in Fig. 2, where the mechanical subsystem has been obtained from the describing equations presented in the previous Section.

Let us first consider the case of a constant generator speed

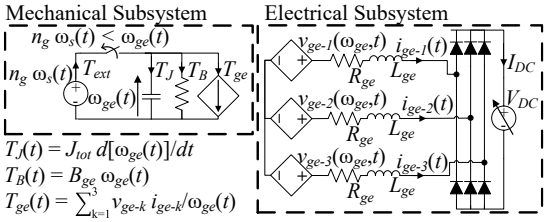

Fig. 2. Equivalent electrical circuit of a TSEH loaded by a diode bridge rectifier.

ω_{ge}, for which (5) reduces to

$$\theta_{ge}(t) = n_p \cdot \omega_{ge} \cdot t \qquad (8)$$

and hence, according to (4), the phase voltages $v_{ge\text{-}k}$ are purely sinusoidal. In the ideal case of null inductance value (L_{ge} = 0) [7], [22] and null diodes voltage drops (V_d = 0), the interval [0, 2π] of $\theta_{ge}(t)$ can be divided in six subintervals of duration π/3 (Fig. 3), wherein only two of the three phases conduct current. These are the ones with the highest and the lowest voltage values. As an example, in the subinterval 1 where $v_{ge\text{-}2}$ is the highest phase voltage and $v_{ge\text{-}3}$ is the lowest one, the electrical subsystem shown in Fig. 2 reduces to that reported in Fig. 4, where the voltage $v_{ge\text{-}23}$, for $\theta_{ge} \in [-\pi/6, \pi/6]$, is given by

$$v_{ge-23}(t) = v_{ge-2} - v_{ge-3} = \sqrt{3}\, k_e\, \omega_{ge}\, cos\left[\theta_{ge}(t)\right] \qquad (9)$$

If the value of V_{DC} ensures the conduction of the diodes, according to Fig. 4, the current in the DC side is

$$I_{DC}(\theta_{ge}) = \frac{v_{ge-23}(\theta_{ge}) - V_{DC}}{2 \cdot R_{ge}} \qquad \forall\theta_{ge} \in \left[-\frac{\pi}{6}, \frac{\pi}{6}\right] \qquad (10)$$

and the instantaneous power is

$$p_{DC}(\theta_{ge}) = \frac{v_{ge-23}(\theta_{ge})\, V_{DC} - V_{DC}^2}{2 \cdot R_{ge}} \quad \forall\theta_{ge} \in \left[-\frac{\pi}{6}, \frac{\pi}{6}\right] \qquad (11)$$

It is possible to obtain the average power delivered to the DC load by averaging (11) over [-π/6, π/6]

$$P_{DC} = \frac{3\sqrt{3} \cdot k_e \cdot \omega_{ge} \cdot V_{DC}}{2 \cdot \pi \cdot R_{ge}} - \frac{V_{DC}^2}{2 \cdot R_{ge}} \qquad (12)$$

Equation (12) shows that the average extracted power is a quadratic function of the DC voltage and an optimal value V_{DC_MPP} of V_{DC} exists, which maximizes the average extracted power. By differentiating (12) with respect to V_{DC} and then equating it to zero, it is possible to find the value of V_{DC_MPP}

$$V_{DC\_MPP} = \frac{1}{2} \cdot \frac{3}{\pi} \cdot \sqrt{3} \cdot k_e \cdot \omega_{ge} = K_{V\_MPP} \cdot \omega_{ge} \qquad (13)$$

Equation (13) shows that V_{DC_MPP} is proportional to ω_{ge} through the constant $K_{V\_MPP} = 0.83 \cdot k_e$. In case that $L_{ge} \neq 0$ and $V_d \neq 0$, (13) still holds with a small error as it will be numerically and experimentally shown in Section V. According to (13), if the measurement of the generator speed ω_{ge} is available in real time, as it is typically available in such kind of applications, it is possible to obtain a real time estimation of the optimal voltage V_{DC_MPP}, which leads to the maximization of the extracted power. This is the principle that is exploited by the

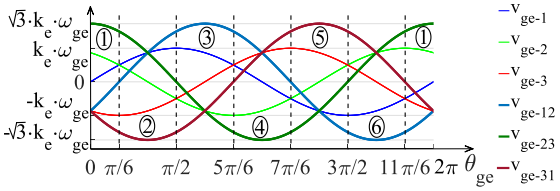

Fig. 3. Six subintervals of $\theta_{ge}(t)$ wherein only two of the three phases conduct.

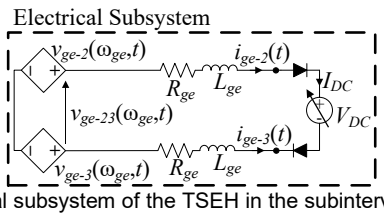

Fig. 4. Electrical subsystem of the TSEH in the subinterval where $v_{ge\text{-}2}$ is the highest phase voltage and $v_{ge\text{-}3}$ is the lowest one.

proposed SDA MPPT technique, and will be described in the next Section.

Note that, the above analysis has been carried out under the assumption of a constant ω_{ge} and, hence, a constant amplitude of $v_{ge\text{-}k}$ in (4). However, (13) is also valid in the case where ω_{ge} varies so slowly that the variation of the amplitude of $v_{ge\text{-}k}$ is negligible during the period $\tau_{ge}(t)$ of such a sinusoidal function, $v_{ge\text{-}k}(t)$. Let us now quantitatively estimate when this condition holds true. Using the first-order approximation of the Taylor series expansion of ω_{ge} it results

$$\omega_{ge}\left(t+\tau_{ge}\right)=\omega_{ge}(t)+\frac{d\omega_{ge}(t)}{dt}\cdot\tau_{ge}(t) \tag{14}$$

The function ω_{ge} is slowly-varying in $\tau_{ge}(t)$ if the condition

$$\omega_{ge}(t)\gg\frac{d\omega_{ge}(t)}{dt}\cdot\tau_{ge}(t) \tag{15}$$

is met. Moreover, by taking into account that

$$\tau_{ge}(t)=\frac{2\pi}{n_p\cdot\omega_{ge}(t)} \tag{16}$$

expression (15) can be rewritten as

$$\omega_{ge}^2(t)\gg\frac{2\pi}{n_p}\cdot\frac{d\omega_{ge}(t)}{dt} \tag{17}$$

Condition (17) can be easily expressed in terms of the TSEH parameters and of the input vibration characteristics in case of sinusoidal input displacement, that is $x(t) = -A_x{\cdot}cos(\omega_x{\cdot}t)$. In the engagement mode, ω_{ge} and $d\omega_{ge}/dt$ can be expressed as

$$\omega_{ge}(t)=\frac{n_g\cdot n_b}{r_p}\cdot A_x\cdot\omega_x\cdot sin(\omega_x\cdot t) \tag{18}$$

$$\frac{d\omega_{ge}(t)}{dt}=\frac{n_g\cdot n_b}{r_p}\cdot A_x\cdot\omega_x^2\cdot\sqrt{1-sin^2(\omega_x\cdot t)} \tag{19}$$

By taking into account (18)-(19), inequality (17) leads to

$$\omega_{ge}^2(t)\gg\omega_x^2\cdot K_\omega(A_x)=$$
$$=\omega_x^2\cdot\left[\frac{1}{2}\sqrt{\left(\frac{2\pi}{n_p}\right)^4+\left(\frac{4\pi n_g n_b A_x}{r_p n_p}\right)^2}-2\left(\frac{\pi}{n_p}\right)^2\right] \tag{20}$$

Inequality (20) identifies a minimum value of the time-varying function $\omega_{ge}(t)$, dependent on the input displacement amplitude and frequency, beyond which the optimal DC voltage V_{DC_MPP} can be still predicted by using (13). Since the time derivative of $\omega_{ge}(t)$ is lower in the disengagement mode (Fig. 1(c)) than that in the engagement mode, if inequality (20) is verified in the engagement mode, then it is also verified in the disengagement mode.

Finally, it is worth noting that since the generator speed changes in real applications due to the time variations of the train suspension vibrations, then according to (13) also V_{DC_MPP} changes with time and needs to be properly tracked.

IV. AC/DC Electronic Interface based on the SDA MPPT Technique

Previous analysis showed that, when a TSEH is loaded by a diode bridge rectifier, the extracted power depends on both the generator speed and the rectifier DC side voltage. Thus, in order to maximize the power extraction, it is necessary to use a DC/DC converter equipped with a MPPT technique which ensures that the value of the DC side voltage, V_{DC}, is as close as possible to the optimal value, V_{DC_MPP}, given by (13).

To this end, a synchronous boost DC/DC converter is placed between the diode bridge rectifier and the DC load (whose voltage V_{LOAD} is nearly constant since it varies with time constants much larger than other quantities in the considered system) to regulate the voltage V_{DC} through a closed-loop feedback, as shown in Fig. 5. This loop is based on a PI regulator, whose input is the error signal between the reference V_{DC_REF} and the measured value of V_{DC}, and whose output is the duty cycle signal of the switches for the PWM modulator. The reference voltage V_{DC_REF} is provided by a MPPT controller, implementing a MPPT technique named SDA and specifically designed for TSEH systems. In particular, by taking into account that V_{DC_MPP} can be estimated by (13), the SDA MPPT controller calculates V_{DC_REF} by multiplying the generator speed ω_{ge}, measured through Hall sensors, by a parameter K_V, i.e.

$$V_{DC\_REF}=K_V\cdot\omega_{ge} \tag{21}$$

According to (13), the extracted power is maximized for K_V equal to K_{V_MPP}. However, K_{V_MPP} can be only known roughly because its value is analytically known only in the ideal case ($L_{ge} = 0$ and $V_d = 0$) and also because its value can change due to the time variations of the controlled system parameters. Hence, the SDA MPPT technique dynamically adapts the parameter K_V in order to make it as close as possible to the optimal value K_{V_MPP}. The operation of the dynamic adaptive algorithm is described in the following.

If the PI closed-loop feedback in Fig. 5 ensures the tracking of V_{DC} to its reference voltage given by (21), (12) reduces to

$$P_{DC}=\frac{3\sqrt{3}\cdot k_e\cdot\omega_{ge}^2\cdot K_V}{2\cdot\pi\cdot R_{ge}}-\frac{K_V^2\cdot\omega_{ge}^2}{2\cdot R_{ge}} \tag{22}$$

and the normalized extracted power is equal to

$$P_{DC\_N}=\frac{P_{DC}}{\omega_{ge}^2}=\frac{3\sqrt{3}\cdot k_e\cdot K_V}{2\cdot\pi\cdot R_{ge}}-\frac{K_V^2}{2\cdot R_{ge}} \tag{23}$$

By differentiating (23) with respect to K_V and then equating it to zero, it is possible to find the value of K_V that maximizes P_{DC_N}

$$\frac{dP_{DC\_N}}{dK_V}=0\quad\rightarrow\quad K_V=\frac{3\sqrt{3}\cdot k_e}{2\cdot\pi}=K_{V\_MPP} \tag{24}$$

Equation (24) shows that the value of K_V that maximizes the normalized extracted power is equal to the desired optimal value K_{V_MPP} introduced in (13). Therefore, the latter one can be determined by looking for the maximization of the normalized power P_{DC_N}. This is a very interesting result which allows us to state that it is possible to determine the optimal value of K_V

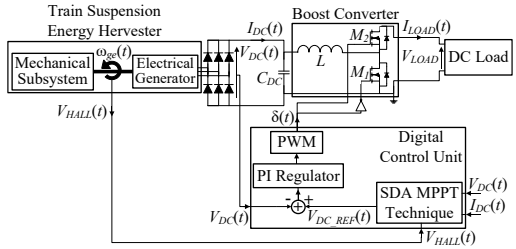

Fig. 5. Train Suspension Energy Harvester loaded with an AC/DC power electronic interface equipped with the proposed SDA MPPT controller.

regardless of the time varying value of the generator speed ω_{ge}.

According to (22)-(24), the SDA MPPT controller implements a perturbative approach to slowly adapt K_V against possible long-time parameter variations. This adaptive control is implemented by periodically giving a perturbation, with a constant amplitude ΔK_V, to the parameter K_V. The sign of the perturbation is updated on the basis of the variation of the normalized power P_{DC_N}, whose value is calculated, as shown in Fig. 6, starting from the measurement of V_{DC}, I_{DC} and ω_{ge}. After a perturbation of K_V, if the corresponding value of P_{DC_N} has increased (decreased), the value of K_V has moved towards (away from) K_{V_MPP}. Therefore, the next perturbation of K_V will have the same (opposite) sign as the previous perturbation and so on. The sign of the perturbation is updated with a period T_K, whose relatively large value is set on the basis of the expected long-time system parameters variations.

The implementation of the Digital Control Unit represented in Fig. 5 is shown in Fig. 6. Its input signals are V_{DC}, I_{DC} and V_{HALL}, and its output is the square-wave control signal for the DC/DC converter switches. The V_{DC} signal is used to implement the inner feedback loop through a PI controller and a PWM modulator, whose digital code is executed at a fast rate in order to ensure a quick dynamic response. The reference voltage V_{DC_REF} is generated according to (21) on the basis of the generator speed, calculated from the output signals V_{HALL} of the Hall sensors. The speed calculation and, hence, the voltage reference updates are performed at every edge of the output signals of the Hall sensors. Since the rate of edges of the Hall sensors is proportional to the generator speed, the execution rate of the last code is variable.

The Dynamic Adaptive Control aimed at updating the value of K_V is implemented at a slow execution rate, i.e. every T_K seconds, because the time variations of K_{V_MPP} are expected to be very slow. As described above, the update of K_V is determined on the basis of the value of the normalized power $P_{DC\_N} = P_{DC}/\omega_{ge}^2$. To this end, P_{DC_N} is calculated at the same fast rate of the PI controller by multiplying the measured values of V_{DC} and I_{DC}, and by dividing the result by ω_{ge}^2. To avoid singularities, the normalized power is evaluated only when ω_{ge} is higher than a specified threshold. Moreover, the highest value of P_{DC_N} during every interval of duration T_K, i.e. $P_{MAX} = max\{P_{DC\_N}\}$, is provided to the Dynamic Adaptive Control every T_K.

It is worth noting that the proposed Dynamic Adaptive Control for K_V, is based on a perturbative approach that falls in the set of "hill climbing" algorithms that also includes the P&O MPPT [28]. For these techniques, the stability and convergence to the maximum value of the objective function is ensured, provided that the maximum is unique and that the "hill climbing" algorithm is designed and customized to the considered application according to the guidelines provided in the literature [28]. Such guidelines require that the update interval T_K must ensure that, after each perturbation of K_V, the system reaches a steady-state condition before the next measurement of the normalized power P_{DC_N} is done. This condition can be easily verified in practice because the expected variations of the system parameters, which are the target of this dynamic adaptation, are characterized by times that are much larger than the system settling time. Moreover, according to the literature stability guidelines, the amplitude perturbation ΔK_V must ensure that the variations of the normalised power P_{DC_N} are greater than the variations of P_{DC_N} due to possible external long-time parameters changes. Also, this condition can be easily met in practical applications.

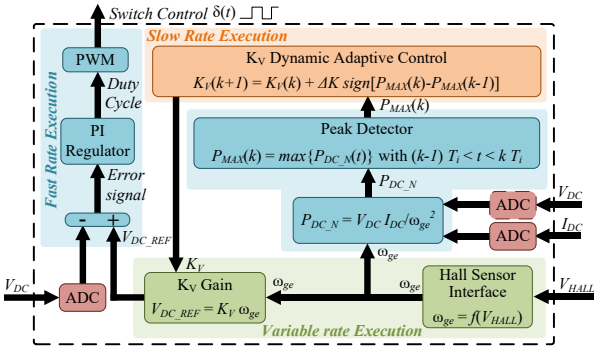

Fig. 6. Schematic representation of the digital control unit implementing the proposed SDA MPPT technique.

In order to design the PI Regulator, a small signal model of the control loop in Fig 5 is developed, by performing an averaging and linearization process around the desired operating point [29]. In Fig. 7(a), $G_{PI}(s)$ is the PI transfer function to be designed, V_{LOAD} is the nearly constant boost converter output voltage, R_L and R_C are the equivalent series resistances of L and C_{DC} respectively. $G_{IV}(s)$ is the V_{DC} to I_{DC} transfer function that models the system at the left of the capacitance C_{DC}. Such a transfer function has been numerically obtained by means of PSIM circuit simulations of the system in Fig. 5. The parameters used for the numerical analysis are reported in Table 1. For the system in Fig. 7(a), it is possible to write the expression of the uncompensated loop gain $T_U(s)$, i.e. by assuming $G_{PI}(s) = 1$,

$$T_U(s) = \frac{V_{BATT} \cdot (1 + s \cdot R_C C_{DC})}{1 - G_{IV}(s) \cdot R_L + s \cdot D_1(s) + s^2 \cdot D_2(s)} \quad (25)$$

$$D_1(s) = C_{DC} \cdot (R_C + R_L) - G_{IV}(s) \cdot (L + R_C R_L C_{DC}) \quad (26.1)$$

$$D_2(s) = L \cdot C_{DC} - G_{IV}(s) \cdot R_C \cdot L \cdot C_{DC} \quad (26.2)$$

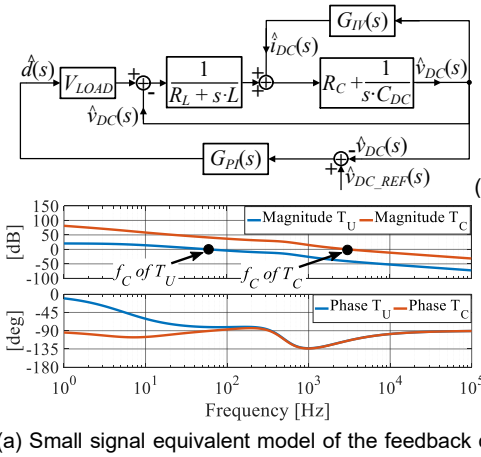

Fig. 7. (a) Small signal equivalent model of the feedback control loop Fig. 5; (b) Bode diagrams of the magnitudes and phases of the transfer functions of T_U and T_C.

By using (25), it is possible to design the transfer function $G_{PI}(s)$ of the PI Regulator leading to a stable closed-loop system with a compensated loop gain $T_C(s) = T_U(s) \cdot G_{PI}(s)$ characterized by an adequate phase margin (65°) and crossover frequency (f_C = 3 kHz = $0.1 \cdot f_S$, where f_S is the switching frequency of the PWM modulator equal to 30 kHz).

The Bode diagrams of the magnitudes and phases of the transfer functions of T_U and T_C, reported in Fig. 7(b), highlight the stability of the closed-loop system and its characteristics in terms of phase margin and crossover frequency.

V. Experimental Results

Experimental results aimed at validating the theoretical analysis and the proposed SDA MPPT technique are reported and discussed in this Section. The parameters of the adopted TSEH are reported in Table 1. With reference to the power electronic interface, shown in Fig. 8, the three-phase diode bridge rectifier has been implemented by means of the passive rectifier legs in the L6205 integrated circuit. The parameters of the DC/DC synchronous boost converter, which has also been implemented by using an active inverter leg in the L6205 integrated circuit, are C_{DC} = 100 µF and L = 100 mH. Since the L6205 integrated circuit allows the operation with a switching frequency up to 100 kHz and the inductor auto-resonance is larger than that frequency, the boost converter switching frequency was set to 30 kHz in order to reduce the switching losses while ensuring acceptable switching ripples. The DC load in Fig. 5 has been substituted by a four quadrant Kepco® power amplifier whose voltage has been set at V_{LOAD} = 15 V. The diode bridge rectifier DC side current I_{DC} has been measured through a resistance $R_{measure}$ = 0.2 Ω and its voltage drop has been filtered and amplified. It is worth noting that in an actual implementation of the system, a real storage element (battery or supercapacitor) should be employed as a DC load. In this case, if it is necessary to slow the dynamics of the entire system in order to optimize the transfer of the energy to the storage element, the inertia of the overall system could be increased. With reference to the digital control unit, the proposed SDA MPPT technique, the PI regulator and the PWM modulator have been implemented in a STM32F401RE microcontroller by STMicroelectronics®. The considered microcontroller, and hence the overall digital control unit, is characterized by a maximum power consumption lower than 80mW.

TABLE 1. Train Suspension Energy Harvester Parameters

Symbol	Parameter	Value
n_b	Bevel Gears Ratio	2
r_p	Pinion Radius	20 mm
k_t	Generator Torque Constant	46.1 mN·m/A
k_e	Generator Voltage Constant	0.0028 V/rpm
B_{ge}	Generator Damping Coefficient	0.15 mNm/rpm
J_{ge}	Generator Moment of Inertia	12.8 g·cm^2
n_p	Number of Generator Pair Poles	7
R_{ge}	Generator Internal Resistance	0.72 Ω
L_{ge}	Generator Internal Inductance	0.57 mH

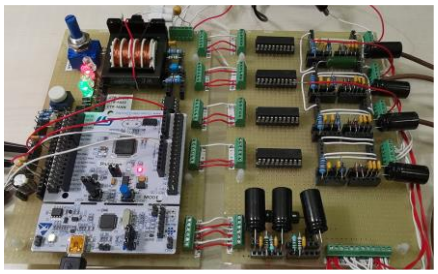

Fig. 8 Picture of the implemented power electronic interface.

A. Harvested power vs. K_V

The first set of tests were carried out in order to validate the main analytical result of Section III, where it has been shown that the optimal DC voltage, V_{DC_MPP}, is proportional through a constant, K_{V_MPP}, to the generator speed, according to (13).

To this end, a number of simulations were performed in PSIM environment by using the same constant generator speed, ω_{ge} = 3300 rpm, and by varying the values of L_{ge}/R_{ge} and V_d, that were set to zero in the theoretical analysis. Results reported in Fig. 9(a) show that, even if the values of L_{ge}/R_{ge} and V_d have a significant impact on the maximum value of the extracted power, their effect on the value of the optimal DC voltage and, hence, of the parameter K_{V_MPP} is less than 15%. Indeed, such optimal values are close to those analytically predicted by (13) with the parameters in Table 1, i.e. V_{DC_MPP} = 7.6 V and K_{V_MPP} = 2.3·mV/rpm. This conclusion is also confirmed by the experimental results, reported in Fig. 9(a) and performed by controlling the DC voltage at the desired testing points.

Furthermore, other experimental tests were performed for different generator speeds. The P_{DC} vs. K_V measured curves are reported in Fig. 9(b) and the MPP voltages of the curves in Fig. 9(b) are reported in Fig. 9(c) as a function of ω_{ge}. These results show the impact of the generator speed on the extracted power and on the values of K_{V_MPP} and V_{MPP}. The generator speed has a significant impact on the maximum value of the extracted power, but its effect on the actual values of K_{V_MPP} and of V_{MPP} is less than 17% with respect to those analytically predicted.

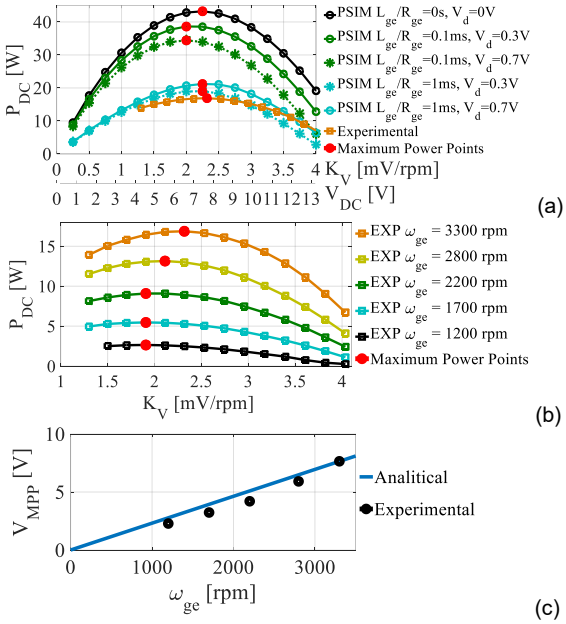

Fig. 9. (a) Simulation (PSIM) and experimental results for ω_{ge} = 3300 rpm; (b) Experimental results for different values of ω_{ge}; (c) Analytical and experimental MPP voltage as a function of ω_{ge}.

The experimental results reported in this section highlight that, on the one hand, the value of K_{V_MPP} analytically predicted by (13) is able to lead to the extraction of a power very close to the MPP in nearly all the considered working conditions while on the other hand, in order to cope with a possible error on the starting value of K_V and with tolerances and time variability of the parameters of the controlled system, a slow adaptation of the value of K_V is needed in order to guarantee that the system extracts always the maximum available power.

B. Tracking ability of the SDA MPPT technique

A second set of experimental tests were carried out in order to show the operation of the proposed SDA MPPT technique and to assess its ability to adjust the value of K_V for tracking the MPP when the generator speed ω_{ge} is constant. To this end, the mechanical part of the TSEH was emulated by means of a DC motor with closed-loop speed controller, driving the real three-phase generator at ω_{ge} = 3300 rpm. The digital control unit implementing the proposed MPPT technique was turned on with a preloaded starting value of K_V equal to 4·mV/rpm, which was intentionally set far from the nominal optimal value predicted by (13), and shown in Fig. 9. Moreover, T_K was set to 5 s, which is a value much lower than the one expected for the parameters' variations, to test the convergence of the adaptive control. In an actual implementation of the system, a greater value of T_K can be selected since the proposed dynamic adaptive control is aimed at facing the tolerances and long-time variabilities of the parameters of the TSEH system. An oscilloscope screenshot is reported in Fig. 10(a) illustrating the tracking process. In order to verify the MPP tracking, a sweep of imposed values for K_V was performed, as shown in Fig. 10(b). By comparing the maximum power extracted in Fig. 10(b) and the steady-state power extracted in Fig. 10(a), it is possible to state that the proposed adaptive control is able to self-adapt the value of K_V in order to track the MPP, even in presence of a significant error in the starting value of K_V.

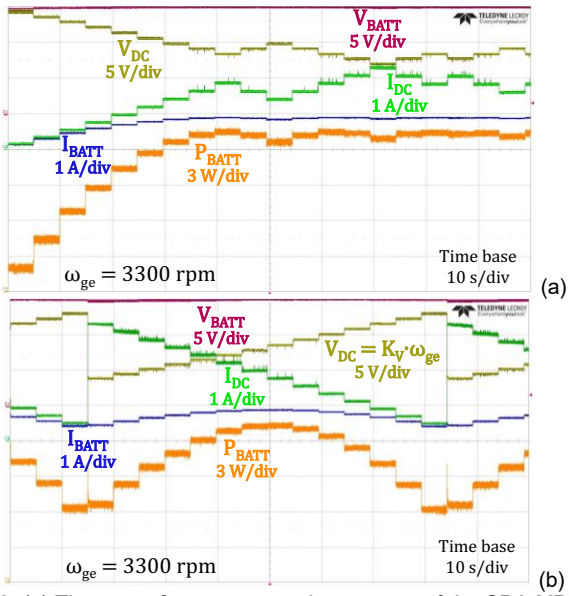

Fig. 10. (a) Time waveforms measured at start-up of the SDA MPPT technique, under a constant ω_{ge} = 3300 rpm. (b) Time waveforms measured during the sweep of K_V with ω_{ge} = 3300 rpm.

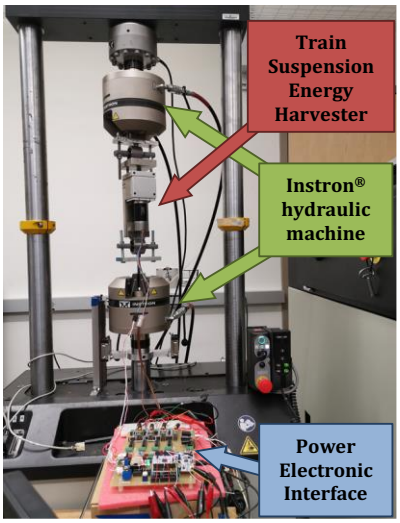

Fig. 11. Picture of the complete experimental set-up.

C. Tests with a real Train Suspension Energy Harvester

The last set of experimental tests were carried out to show the operation of the proposed SDA MPPT technique when applied to a real TSEH. To this end, the proposed power electronic interface was connected to a prototype of the TSEH in Fig. 1 mounted on an Instron® hydraulic test machine, as shown in Fig. 11. The lower grip of the Instron® machine was rigidly connected with the hydraulic actuator controlled by a built-in software. A National Instrument® acquisition board was used to record the three phases AC voltages and the voltage and current at the output of the diode bridge rectifier.

Firstly, the TSEH with the proposed power electronic interface was tested under a sinusoidal excitation with a vibration frequency f_x = 2 Hz ($\omega_x = 2{\cdot}\pi{\cdot}f_x$) and a vibration amplitude A_x = 3 mm. This sinusoidal displacement is transformed by the MMR with transmission ratio n_g = 66 in a nearly half sinusoidal generator speed $\omega_{ge}(t)$ with a peak value $\omega_{ge\text{-}MAX}$ equal to about 2380 rpm. Since, for the considered system, K_ω = 17.4 and $\sqrt{K_\omega}{\cdot}\omega_x$ = 500 rpm, inequality (20) is verified and therefore the optimal DC voltage V_{DC_MPP} can be estimated by (13).

The imposed displacement, the three phases AC voltages, the DC voltage V_{DC} and the power provided at the output of the bridge rectifier P_{DC} obtained by employing the SDA MPPT technique are reported in Fig. 12(a). Moreover, a zoomed-in image of the voltages v_{ge} inside the red square in Fig. 12(a) is shown in Fig 12(b). The waveforms show that the proposed electronic interface dynamically adapts the DC voltage proportionally to the generator speed for tracking the MPP. The average extracted power is $P_{DC\text{-}SDA}$ = 7.3 W.

The performance of the proposed SDA MPPT technique was compared with the conventional P&O MPPT algorithm. To ensure a fair comparison, the system in Fig. 5 was also implemented with a P&O algorithm providing the reference voltage for V_{DC}. The values of the update time interval $T_{P\&O}$ and the amplitude of the voltage perturbation ΔV_{DC_REF} were determined by carrying out some preliminary experimental tests. The resulting best values of such parameters came out to

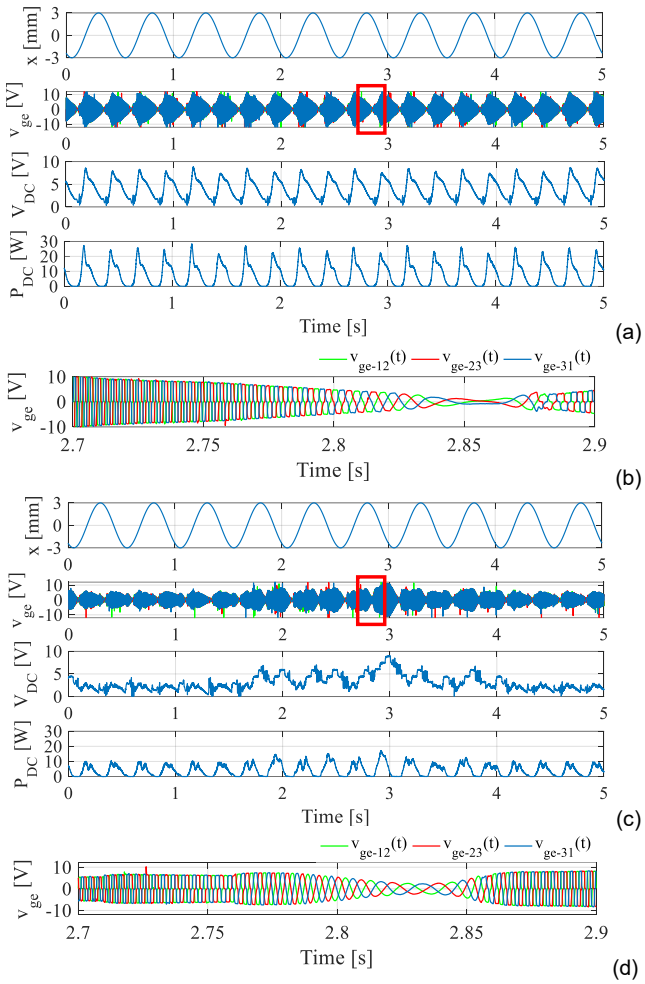

Fig. 12. Time waveforms measured when the harvesting system is driven by a sinusoidal excitation 2Hz and 3mm. (a) SDA MPPT and (b) zoom of v_{ge} inside the red square in Fig. 12(a); (c) P&O MPPT and (d) zoom of v_{ge} inside the red square in Fig. 12(c).

be $T_{P\&O} = 0.05$ s and $\Delta V_{DC\_REF} = 1.5$ V. The signals recorded by employing the P&O MPPT technique under the above sinusoidal excitation are reported in Fig. 12(c), and the zoomed-in image of the voltages v_{ge} inside the red square are shown in Fig. 12(d). The waveforms show that the P&O leads to a DC voltage that allows a lower extracted power, $P_{DC\text{-}P\&O} = 4.9$ W. Hence, the proposed SDA MPPT technique leads to a percent gain $\Delta P\% = (P_{DC\text{-}SDA}/P_{DC\text{-}P\&O} - 1)\%$ equal to about 49 % with respect to the usual P&O technique.

The results of a second set of experimental tests with a sinusoidal excitation with vibration frequency $f_x = 3$ Hz and vibration amplitude $A_x = 2$ mm are also reported. The waveforms obtained by the SDA technique reported in Fig. 13(a) confirm the ability to track the MPP; the average extracted power is $P_{DC\text{-}SDA} = 5.6$ W. The waveforms obtained by the P&O are reported in Fig. 13(b) with an average extracted power $P_{DC\text{-}P\&O} = 3.7$ W. The above results confirm that the proposed SDA technique leads to a better performance with a percent gain $\Delta P\%$ equal to about 51 %.

The proposed system was also tested with the harvester forced by a train suspension displacement $x(t)$ equal to that recorded on a freight railcar running on an operational track [7].

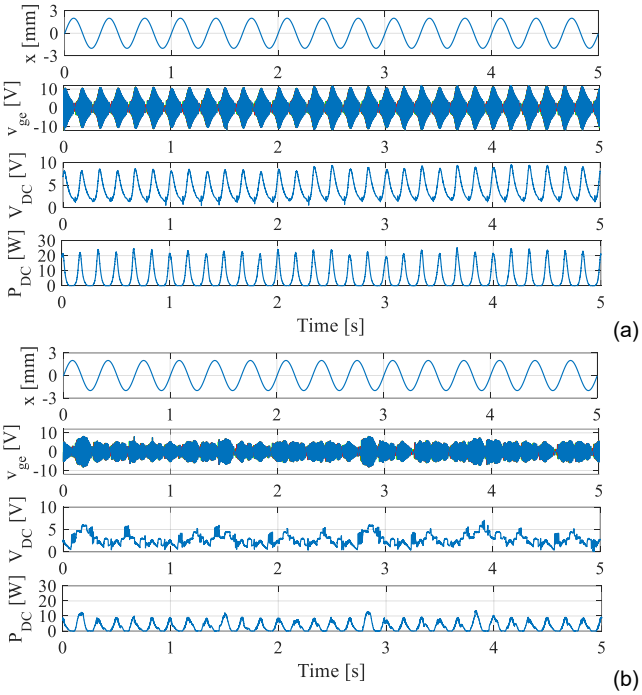

Fig. 13. Time waveforms measured when the harvesting system is driven by a sinusoidal excitation 3Hz and 2mm. (a) SDA MPPT and (b) P&O MPPT.

In the lab tests, the vibration amplitude was reduced to one half resulting in a peak amplitude of $x(t)$ equal to 3 mm and an RMS value equal to about 0.9 mm, as shown in Fig. 14(a). The FFT amplitude, reported in Fig. 15 for the signal $x(t)$, shows that the main frequency content is localized around few hertz. The results of these tests are reported in Fig. 14 both for the SDA technique and for the P&O technique. The recorded signals show that the SDA technique is able to perform well even in presence of an actual on-field time-variable displacement and that, it is able to extract an average power much higher than the P&O technique, leading to a gain $\Delta P\% = 57$ %.

It is worth noting that the results obtained here are coherent with those reported in [7], where the TSEH was tested with a recorded train suspension displacement having a peak value equal to 6 mm and with a resistive load. In fact, for a fair comparison, as the power is roughly proportional to the square of the displacement amplitude, the extracted power measured in [7] should be reduced to 25% due to the halved displacement amplitude. The resulting power should be further reduced to about 70% when substituting a resistive load with a loss-less rectifying load, as shown in [21]. Finally, it should be further reduced to around 70% for the converter losses.

A summary of the results obtained in all the tests is reported in Table 2, in order to highlight the comparison between the power extracted with the proposed SDA technique and with the widely-used P&O technique. The results show that the

TABLE 2. EXTRACTED POWER FOR DIFFERENT INPUT DISPLACEMENTS.

Input Displacement	Average $P_{DC\text{-}SDA}$ SDA MPPT	Average $P_{DC\text{-}P\&O}$ P&O MPPT	$\Delta P\%$
Sinusoidal (3mm – 2 Hz)	7.3 W	4.9 W	49 %
Sinusoidal (2mm – 3 Hz)	5.6 W	3.7 W	51 %
On-field	1.1 W	0.7 W	57 %

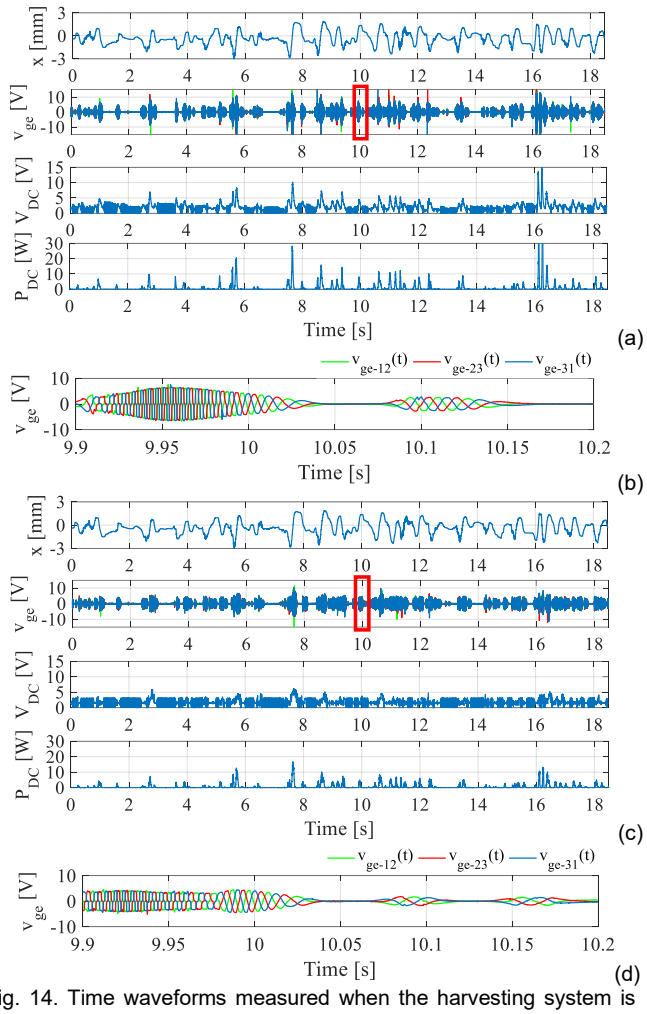

Fig. 14. Time waveforms measured when the harvesting system is driven by a train suspension displacement recorded on a freight railcar running on an operational track. (a) SDA MPPT and (b) zoom of v_{ge} inside the red square in Fig. 14(a); (c) P&O MPPT and (d) zoom of v_{ge} inside the red square in Fig. 14(c).

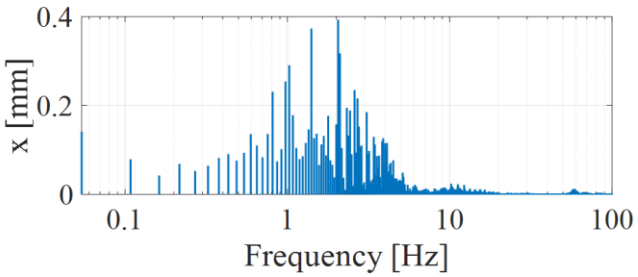

Fig. 15. FFT amplitude of the signal *x* of Fig. 14.

proposed technique exhibits significantly better performance with respect to the state-of-the-art technique, both in case of sinusoidal displacement (3mm – 2 Hz and 2mm – 3 Hz) and in case of a real train suspension displacement.

Note that the extracted power in case of sinusoidal displacements is larger than that measured in case of real displacement, because in the former cases the amplitudes are equal to 2mm and 3mm, while in the latter case the displacement peak value in the frequency spectrum (Fig. 15) is lower than 0.4 mm and the RMS value is about 0.9 mm.

It is worth noting that, also in case of real displacements, the average power extracted from the TSEH loaded by the proposed electronic interface is high enough to power the wireless sensor networks for onboard monitoring of railway freight wagons [30].

Finally, a comparison of the proposed TSEH equipped with the SDA MPPT technique with other vibration energy harvesting systems with MPPT published in the literature is reported in Table 3. It emerges that MPPT techniques for vibration energy harvesters are used in very heterogeneous applications that differ for the extracted power (from mW [24], [31]-[34], [36] to W [35] as in this paper), for the harvester type (resonant [24], [31]-[34] or non-resonant [35]-[36] as in this paper), for the transducer type (piezoelectric [31]-[34] or electromagnetic [24], [35]-[36] as in this paper) and for the characteristics of the source of vibrations. In the authors knowledge, the proposed one is the first implementation of a MPPT technique for a TSEH system, specifically designed and optimized for railway applications.

VI. Conclusions

The proposed power electronic interface equipped with the SDA MPPT technique is effective in maximizing the power extracted from train suspension energy harvesters, driven by rapidly varying vibrations. In these operating conditions that are typical in railway applications, the widely-used Perturb and Observe technique is not able to reach and follow the maximum power point due to its blind and step-by-step operation. By exploiting the measurement of the harvester generator speed, the SDA technique on the other hand is able to almost instantaneously predict the maximum power point. Moreover, the proposed technique does not require an accurate design of the algorithm parameters, as the Perturb and Observe technique, because it implements an adaptive control to deal with tolerances and time variability of the parameters of the controlled system. Experimental results confirm the theoretical predictions and the better performance of the SDA compared with the Perturb and Observe technique. Future research will be devoted to investigate and optimize the system performance when the energy is stored into a rechargeable battery or into a supercapacitor.

References

[1] Y. Zhang, K. Guo, D. Wang, C. Chen, X. Li, “Energy conversion mechanism and regenerative potential of vehicle suspensions,” *Energy*, vol. 119, no., pp. 961–970, Jan. 2017.

[2] L. Li, Y. Zhang, C. Yang, B. Yan, C.M. Martinez, “Model predictive control-based efficient energy recovery control strategy for regenerative braking system of hybrid electric bus,” *Energy Conversion and Management*, vol. 111, no., pp. 299–314, Mar. 2016.

[3] M.A.A. Abdelkareem, L. Xu, M.K.A. Ali, A. Elagouz, J. Mi, S. Guo, Y. Liu, L. Zuo, “Vibration energy harvesting in automotive suspension system: A detailed review,” *Applied Energy*, vol. 229, pp. 672-699, 2018.

[4] L. Zuo, B. Scully, J. Shestani, Y. Zhou, “Design and characterization of an electromagnetic energy harvester for vehicle suspensions,” *Smart Mater Struct*, vol. 19, no. 4, pp. 045003, Feb. 2010.

[5] B. Sapiński, S. Krupa, “Efficiency improvement in a vibration power generator for a linear MR damper: numerical study,” *Smart Mater Struct*, vol. 22, no. 4, pp. 045011, Mar. 2013.

[6] C. Nagode, M. Ahmadian, S. Taheri, “Effective energy harvesting devices for railroad applications,” in *Proc. SPIE, Act and Pass Smart Struc and Integ Sys*, vol. 7643, pp., Apr. 2010.

TABLE 3. COMPARISON OF VIBRATION ENERGY HARVESTING SYSTEMS EQUIPPED WITH MPPT.

	[31]	[32]	[33]	[34]	[24]	[35]	[36]	This Work
Harvester Type	Resonant	Resonant	Resonant	Resonant	Resonant	Non-resonant	Non-resonant	Non-resonant
Transducer Type	Piezoelectric	Piezoelectric	Piezoelectric	Piezoelectric	Electromagnetic	Electromagnetic	Electromagnetic	Electromagnetic
Vibrations Shape	Sinusoidal	Sinusoidal	Sinusoidal	Sinusoidal	Amplitude Modulated	Amplitude Modulated	Non-sinusoidal	Non-sinusoidal
Vibration Characteristics	Acceleration 0.5 g	OC voltage 25 V *	OC voltage 12V *	OC voltage 45 V *	Acceleration 0.5 g–2 g	n/a	Acceleration 0.08 g RMS	Displacement 0.9 mm RMS
Main frequency	47 Hz	50 Hz	18 Hz	53.8 Hz	150 Hz	110 Hz–170 Hz	≈ 1.5 Hz	≈ 2 Hz
MPPT Technique	P&O	OCV	OCV	P&O	P&O	P&O	OCV	SDA
Extracted Power	8.4 mW	19.5 mW	0.35 mW	13 mW	1.95 mW	7.96 W	0.225 mW	On-field 1.1 W Sin 7.3 W

* In the paper, vibration characteristics are defined through the Open Circuit (OC) voltage of the harvester.

[7] Y. Pan, F. Liu, R. Jiang, Z. Tu, L. Zuo, "Modeling and onboard test of an electromagnetic energy harvester for railway cars," *Applied Energy*, vol. 250, no., pp. 568-581, Sep. 2019.

[8] A. Pourghodrat, C.A. Nelson, S.E. Hansen, V. Kamarajugadda, S.R. Platt, "Power harvesting systems design for railroad safety," in *Proc Instit Mech Eng Part F: J Rail Rapid Transit*, vol. 228, no. 5, pp. 504–521, Apr. 2013.

[9] A. Pourghodrat, C.A. Nelson, K.J. Phillips, M. Fateh, "Improving an energy harvesting device for railroad safety applications," in *Proc. SPIE, Act and Pass Smart Struc and Integ Sys*, vol. 7977, pp., Apr. 2011.

[10] A. Pourghodrat, C.A. Nelson, "A system for generating electricity using the passage of train wheels for improving railroad track safety," in *Proc. ASME Int. Des. Eng. Tech. Conf. and Comp. and Inf. in Eng. Conf.*, vol. 4, pp. 1025-1031, Aug. 2012.

[11] J.J. Wang, G. Penamalli, L. Zuo, "Electromagnetic energy harvesting from train induced railway track vibrations," in *Proc. of IEEE/ASME Int. Conf. on Mech. and Emb. Sys. and Appl.*, vol., pp. 29–34, Aug. 2012.

[12] X. Zhang, Z. Zhang, H. Pan, W. Salman, Y. Yuan, Y. Liu, "A portable high-efficiency electromagnetic energy harvesting system using supercapacitors for renewable energy applications in railroads," *Energy Convers Manage*, vol. 118, no., pp. 287–294, Jun. 2016.

[13] X. Zhang, H. Pan, L. Qi, Z. Zhang, Y. Yuan, Y. Liu, "A renewable energy harvesting system using a mechanical vibration rectifier (MVR) for railroads," *Applied Energy*, vol. 204, no., pp. 1535–1543, Oct. 2017.

[14] J. Wang, T. Lin, L. Zuo, "High efficiency electromagnetic energy harvester for railroad application," in *Proc. of ASME 2013 Int. Des. Eng. Tech. Conf. and Comp. and Inf. in Eng. Conf.*, vol., pp., Aug. 2013.

[15] T. Lin, J.J. Wang, L. Zuo, "Efficient electromagnetic energy harvester for railroad transportation," *Mechatronics*, vol. 53, pp. 277–286, Aug. 2018.

[16] T. Lin, Y. Pan, L. Zuo, "Dynamics modeling of train-track-harvester system and in-field testing of railroad energy harvester," in *Proc. of ASME 2016 Dyn. Sys. and Cont. Conf.*, vol., pp., Oct. 2016.

[17] T. Lin, Y. Pan, S. Chen, L. Zuo, "Modeling and field testing of an electromagnetic energy harvester for rail tracks with anchorless mounting," *Applied Energy*, vol. 213, no., pp. 219–226, Mar. 2018.

[18] J. Dicken, P.D. Mitcheson, I. Stoianov, E.M. Yeatman, "Power-extraction circuits for piezoelectric energy harvesters in miniature and low-power applications," *IEEE Trans. Power Electron.*, vol.27, pp. 4514-4528, 2012.

[19] S. Du, et all., "A Passive Design Scheme to Increase the Rectified Power of Piezoelectric Energy Harvesters," *IEEE Trans. on Ind. Electron.*, vol. 65, no. 9, pp. 7095-7105, Sept. 2018.

[20] R. D'hulst, et al., "Power Processing Circuits for Piezoelectric Vibration-Based Energy Harvesters," *IEEE Trans. Ind. Electron.*, vol. 57, no. 12, pp. 4170-4177, Dec. 2010.

[21] L. Costanzo, M. Vitelli, Y. Pan, L. Zuo, "Maximizing the Power Extraction From Train Suspension Energy Harvesting System," in Proc. of the ASME 2019 Int. Des. Eng. Tech. Conf. and Comp. and Inf. in Eng. Conf., vol. 8, pp., Aug. 2019.

[22] L. Costanzo, A. Lo Schiavo, M. Vitelli, "Power Extracted from Piezoelectric Harvesters Driven by Non-Sinusoidal Vibrations," *IEEE Trans. on Circ. and Sys. I: Reg. Papers.*, vol. 66, pp. 1291-1303, 2019.

[23] L. Costanzo, A. Lo Schiavo, M. Vitelli, "Power maximization from resonant electromagnetic vibration harvesters feeding bridge rectifiers," *Int J Circ Theor Appl.*, vol. 47, no. 1, pp. 87-102, Jan. 2019.

[24] L. Costanzo, A. L. Schiavo, M. Vitelli, "Design Guidelines for the Perturb and Observe Technique for Electromagnetic Vibration Energy Harvesters Feeding Bridge Rectifiers," *IEEE Trans. on Ind. Appl.*, vol. 55, no. 5, pp. 5089-5098, Sept.-Oct. 2019.

[25] M. Balato, L. Costanzo, A. Lo Schiavo, M. Vitelli, "Optimization of both Perturb & Observe and Open Circuit Voltage MPPT Techniques for Resonant Piezoelectric Vibration Harvesters feeding bridge rectifiers," *Sens. and Act. A: Physical*, vol. 278, no., pp. 85-97, Aug. 2018.

[26] L. Costanzo, A. L. Schiavo and M. Vitelli, "Active Interface for Piezoelectric Harvesters Based on Multi-Variable Maximum Power Point Tracking," *IEEE Trans. on Circ. and Sys. I: Reg. Papers* .

[27] Z. Li, L. Zuo, J. Kuang, G. Luhrs, "Energy-harvesting shock absorber with a mechanical motion rectifier", *Smart Mat. and Struct.*, vol. 22, no. 2, pp. 025008, Dec. 2012.

[28] N. Femia, G. Petrone, G. Spagnuolo and M. Vitelli, "Optimization of perturb and observe maximum power point tracking method," in IEEE Transactions on Power Electronics, vol. 20, no. 4, pp. 963-973, July 2005.

[29] R. W. Erickson and D. Maksimovic, Fundamental of Power Electronics. Norwell, MA: Kluwer, 2001.

[30] A. Lo Schiavo, "Fully Autonomous Wireless Sensor Network for Freight Wagon Monitoring," *IEEE Sensors Journal*, vol. 16, no. 24, pp. 9053-9063, 15 Dec.15, 2016.

[31] N. Kong and D. S. Ha, "Low-Power Design of a Self-powered Piezoelectric Energy Harvesting System With Maximum Power Point Tracking," in IEEE Transactions on Power Electronics, vol. 27, no. 5, pp. 2298-2308, May 2012, doi: 10.1109/TPEL.2011.2172960.

[32] G. Shi et al., "An Efficient Power Management Circuit Based on Quasi Maximum Power Point Tracking With Bidirectional Intermittent Adjustment for Vibration Energy Harvesting," in IEEE Transactions on Power Electronics, vol. 34, no. 10, pp. 9671-9685, Oct. 2019, doi: 10.1109/TPEL.2019.2892457.

[33] Wen, Fengjie, et al. "Hysteresis controlled MPPT for piezoelectric energy harvesting." IEICE Electronics Express 17.2 (2020): 20190722-20190722.

[34] G. K. Ottman, H. F. Hofmann, A. C. Bhatt and G. A. Lesieutre, "Adaptive piezoelectric energy harvesting circuit for wireless remote power supply," in IEEE Transactions on Power Electronics, vol. 17, no. 5, pp. 669-676, Sept. 2002, doi: 10.1109/TPEL.2002.802194.

[35] K. H. Tse and H. S. Chung, "MPPT for Electromagnetic Energy Harvesters Having Nonnegligible Output Reactance Operating Under Slow-Varying Conditions," in IEEE Transactions on Power Electronics, vol. 35, no. 7, pp. 7110-7122, July 2020, doi: 10.1109/TPEL.2019.2959625.

[36] M. Carandell, D. M. Toma, M. Carbonell, J. del Rio and M. Gasulla, "Design and Testing of a Kinetic Energy Harvester Embedded into an Oceanic Drifter," in IEEE Sensors Journal, doi: 10.1109/JSEN.2020.2976517.

Luigi Costanzo was born in Villaricca (Napoli), Italy, in 1989. He received the Master's Degree (cum laude) in Electronic Engineering from the Second University of Naples, Italy, in 2014. He received the Ph.D degree in Energy Conversion from the Department of Industrial and Information Engineering (DIII) of Università degli Studi della Campania "Luigi Vanvitelli", in 2017.
He is currently a Research Fellow at the Department of Engineering of Università degli Studi della Campania "Luigi Vanvitelli". His main research interests include maximum power point tracking techniques in photovoltaic applications; power electronics circuits for renewable energy sources; methods for analysis and design of switching converters; methods to harvest and store energy from any available source.

Teng Lin was born in Qingdao, China, in 1989. He received his B.S. (magna cum laude), M.S. and Ph.D. degree in Mechanical Engineering, from Stony Brook University, NY, in 2012 and 2018. He is currently working in industry and holding an adjunct lecturer position in New York Institute of Technology. His main research interests include energy harvesting, vibration analysis and control, mechatronics design, and pharmaceutical manufacturing.

Weihan Lin received Bachelor of Science in Mechanical Engineering from Virginia Tech, in 2019.
He is currently working towards his M.S. degree in mechanical engineering in Virginia Tech. His main research interests include vibration energy harvesting, ocean energy conservation and machine learning.

Alessandro Lo Schiavo (M'99) was born in Naples, Italy, in 1972. He received the Laurea degree (cum laude) in Electronic Engineering from the Università degli Studi di Napoli, Naples, Italy, in 1997, and the Ph.D. degree from the Seconda Università degli Studi di Napoli, Naples, Italy, in 2000.
From 2001 to 2017 he was Assistant Professor at the Dipartimento di Ingegneria dell'Informazione, Seconda Università degli Studi di Napoli, Italy. In 2017 he was appointed Associate Professor of Electronics at the Università degli Studi della Campania "Luigi Vanvitelli", Italy, where he teaches fundamentals of microelectronics and design of electronic circuits. His current research interests are in the areas of electronic circuits for energy harvesting, wireless sensor networks, analysis and design of analog circuits, and nonlinear circuit theory.

Massimo Vitelli was born in Caserta, Italy, in 1967. He received the laurea degree (cum laude) in electrical engineering from the University of Naples Federico II, Naples, Italy, in 1992.
He is currently a Full Professor with the Department of Engineering, Università degli Studi della Campania "Luigi Vanvitelli," where he teaches electro technics and power electronics. He has been engaged in many scientific national projects. He has co-authored 14 national and international patents. His main research interests include maximum power point tracking techniques in photovoltaic applications, power electronics circuits for renewable energy sources, and methods for analysis and design of switching converters. He is an Associate Editor of the IEEE Transactions on Power Electronics.

Dr. Lei Zuo is the Robert E. Hord Jr. Professor at Virginia Tech and the Director of the NSF Industry-University Cooperative Research Center for Energy Harvesting Materials and Systems (CEHMS). His research interest includes design, dynamics, control, and manufacturing of energy systems, with applications to marine energy conversion, vibration energy harvesting, and self-powered control and sensing. He has authorized about 300 research papers and has advised 15 Ph.D. and over 40 masters to competition of their degrees. He was the sole recipient of the 2017 ASME Leonardo Da Vinci Award and the 2015 ASME Thar Energy Design Award. He also won two R&D 100 Awards by R&D Magazine in 2015 and 2011, and Ralph R. Teetor Educational Award by SAE in 2014. He completed his B.S. from Tsinghua University in 1997, two M.S. and Ph.D. degrees from MIT in 2002 and 2005. He is a Fellow of ASME.